fire

MDPI

Article

Experimental and Numerical Simulation Study of the Influence of $Fe(C_5H_5)_2$-SiO_2 Composite Dry Powders on Characteristics of Hydrogen/Methane/Air Explosion

Zhiqian Zheng [1], Huiqian Liao [1], Hongfu Mi [1,2,*], Kaixuan Liao [1], Haoliang Zhang [1], Yi Li [1], Yanhui Ren [3], Zhijun Li [1], Nanfang Li [1] and Wei Xia [3]

[1] College of Safety Engineering, Chongqing University of Science and Technology, Chongqing 401331, China; michaelqzheng@163.com (Z.Z.); 2023207045@cqust.edu.cn (H.L.); 2022207013@cqust.edu.cn (K.L.); 2022207021@cqust.edu.cn (H.Z.); 2023207018@cqust.edu.cn (Y.L.); 2008044@cqust.edu.cn (Z.L.); 2023207014@cqust.edu.cn (N.L.)
[2] Chongqing Key Laboratory for Oil and Gas Production Safety and Risk Control, Chongqing 401331, China
[3] Northeast Sichuan Gas Mine, Southwest Oil and Gas Field Branch, PetroChina Company Limited, Dazhou 635002, China; oasiaflash@outlook.com (Y.R.); 983755801@foxmail.com (W.X.)
* Correspondence: mimihh5@163.com

Abstract: In order to ensure the safety of methane/hydrogen, regular SiO_2 powder was modified. $Fe(C_5H_5)_2/SiO_2$ composite dry powder (CDP) was selected as the explosion-suppression material. Explosion-suppression experiments and numerical simulations were adopted to investigate the inhibition effect of 0% (X_{H_2} = 0%) and 20% (X_{H_2} = 20%) hydrogen doping ratios. The flame structure, flame propagation speed, and maximum explosion pressure are depicted to compare the inhibition effect of different mass fractions ($X_{Fe(C5H5)2}$ = 0–6%). The results showed that CDP significantly reduced the flame propagation velocity and maximum explosion pressure of X_{H_2} = 0%. The best effect was observed when 6% $Fe(C_5H_5)_2$ was added, with the velocity reduced to 9.241 m/s. The maximum explosion pressure was reduced to 0.518 MPa, and the effect was relatively weak for X_{H_2} = 20%, with the maximum pressure reduced to 0.525 MPa. In addition, the key radical production and temperature sensitivity showed that $Fe(C_5H_5)_2$ altered the molar fractions of the major species and increased the consumption of •H, •O, and •OH. As the mass fraction of $Fe(C_5H_5)_2$ increased, the steady-state concentrations of •H, •O, and •OH in the system showed a significant decreasing trend. This phenomenon originated from the two-step synergistic mechanism of $Fe(C_5H_5)_2$ inhibiting radical generation and accelerating radical consumption. This study provides insight into the process of $Fe(C_5H_5)_2/SiO_2$ composite dry powder inhibition and renders theoretical guidance for the explosion protection of methane/hydrogen.

Keywords: hydrogen/methane/air; composite powders; explosion inhibition; reaction mechanism

check for updates

Academic Editor: Huaming Dai

Received: 23 April 2025
Revised: 7 May 2025
Accepted: 12 May 2025
Published: 15 May 2025

Citation: Zheng, Z.; Liao, H.; Mi, H.; Liao, K.; Zhang, H.; Li, Y.; Ren, Y.; Li, Z.; Li, N.; Xia, W. Experimental and Numerical Simulation Study of the Influence of $Fe(C_5H_5)_2$-SiO_2 Composite Dry Powders on Characteristics of Hydrogen/Methane/Air Explosion. *Fire* **2025**, *8*, 198. https://doi.org/10.3390/fire8050198

Copyright: © 2025 by the authors. Licensee MDPI, Basel, Switzerland. This article is an open access article distributed under the terms and conditions of the Creative Commons Attribution (CC BY) license (https://creativecommons.org/licenses/by/4.0/).

1. Introduction

Hydrogen energy, as a clean and efficient renewable energy carrier, serves as a pivotal bridge between conventional fossil fuels and emerging sustainable energy systems [1,2]. The most technologically viable application currently involves blending hydrogen into natural gas, which enables its efficient transportation through existing natural gas pipeline infrastructures [3]. However, this hydrogen/methane mixture introduces elevated safety risks compared to pure methane due to hydrogen's lower ignition energy and broader

flammability range, presenting substantial challenges to conventional explosion mitigation techniques [4–6]. Consequently, priority should be given to controlling explosion intensity. Mitigating explosion risks is critical for safe methane/hydrogen mixture applications.

The present focus of research on hydrogen/methane explosion suppression materials is on inert gas, water mist, powder, porous materials, and fluorides. Among them, powders are extensively applied in explosion suppression systems, owing to their operational efficiency, storage convenience, and eco-friendly characteristics. A novel multicomponent inhibitor was synthesized via the combination of ammonium polyphosphate (APP), aluminium hydroxide (ATH), and porous-structured kaolinite [7]. The composite powder demonstrated superior explosion-suppression efficiency. Physical barrier formation and endothermic decomposition were identified as dominant suppression mechanisms. Liang [8] prepared a composite powder of $KHCO_3$ and modified slag by employing the mechanochemical technology. The findings demonstrate that the composite powder shows a superior explosion suppression compared to its separate constituents. Additionally, the study elucidated the physical and chemical inhibition mechanisms of the composite powder. Xiao [9] prepared KH_2PO_4/montmorillonite composite powders by the solvent–antisolvent method, utilizing montmorillonite as a carrier and KH_2PO_4 as a loading particle. The results showed that the flame propagation was effectively mitigated when the inert ratio of the KH_2PO_4/montmorillonite composite powder was 1.2, and the explosion was largely suppressed when the inert ratio was 1.8. Krasnyansky [10] developed a composite powder to inhibit methane/air explosion by using urea, potassium chloride, and a small amount of atomized silicon dioxide. The results showed that the material had a good synergistic inhibition effect and a good detonation inhibition effect. Yu [11] added an appropriate amount of $Fe(C_5H_5)_2$ and grinding in potassium bicarbonate to prepare the composite powder and studied its suppression effect on methane explosion. The addition of $Fe(C_5H_5)_2$ considerably increased hydrophobicity and reduced the hygroscopicity and aggregation of composite powder, thus improving the pyrolysis performance of the inorganic salt powder. A test [12] was conducted by Jia to study the efficacy of APP–diatomite composite powder in preventing methane/coal dust compound explosions. The findings indicate that the composite powder exhibits the most effective explosion suppression. Yan [13] prepared a composite ultrafine ABC dry powder containing ferrocene and found that the fire-extinguishing effect was better after adding $Fe(C_5H_5)_2$. It can be ascertained from the existing literature that the composite powder material, for explosion suppression efficiency, is better than a single powder material. Therefore, based on the coupling mechanism of physical explosion suppression and chemical explosion suppression, the use of two or more different properties of the explosion-suppression materials to develop a new type of high-efficiency explosion-suppression agent has great potential and prospects for application.

The iron-containing compounds have been identified as the most effective [14] in flame suppression, which has led to a great deal of interest from scholars in this area. It [15–17] has been demonstrated that iron pentacarbonyl is highly effective in flame suppression, while also exhibiting considerable toxicity. In recent years, Rausch [18] has discovered $Fe(C_5H_5)_2$, an iron-containing compound, as a potential alternative to iron pentacarbonyl due to its excellent flame suppression efficiency [15,19–21]. $Fe(C_5H_5)_2$, a prototypical organometallic iron-based compound, demonstrates exceptional efficacy in combustion modulation and energy applications. The cyclopentadienyl ligands in its molecular architecture synergize with the iron core to efficiently scavenge key radical intermediates (e.g., •H and •OH) during chain-branching combustion reactions, exhibiting a 1.8-fold higher quenching efficiency compared to Fe_3O_4 nanoparticles. Furthermore, ferrocene's unique intercalation capability enables uniform dispersion on SiO_2 carriers via

solvent-assisted methods, achieving nanoscale homogeneity with a marked improvement over $FeCl_3$-derived materials prone to severe aggregation. Accordingly, $Fe(C_5H_5)_2$ was identified as the explosion-suppression material to complement $Fe(C_5H_5)_2$ research in the area of hydrogen–methane mixture explosion. Furthermore, in order to enhance the inhibition ability of the powder, an environmentally friendly material with a high melting point and boiling point, as well as an economical price, SiO_2, was selected as the inert component.

This study investigated the suppression characteristics and reaction mechanisms of $Fe(C_5H_5)_2$ composite powder on hydrogen/methane/air mixture explosions through experiments and numerical simulations. Through experiments, the flame structure, flame propagation velocity, and explosion pressure were analyzed under different hydrogen concentrations with varying proportions of composite powder, evaluating the suppression effects on hydrogen/methane/air mixture explosions under various conditions. The temperature sensitivity coefficient was further analyzed. Additionally, numerical simulations were conducted on key free radicals in hydrogen/methane/air mixture explosions with $Fe(C_5H_5)_2$ addition to enhance the understanding of inhibition kinetics.

2. Experimental and Numerical Methods

2.1. Materials and Preparation

In this study, $Fe(C_5H_5)_2$ and SiO_2 were used as raw materials. First, the powders were accurately weighed in specific volume ratios. This was followed by homogenization using a high-speed mixer with a parameter setting of 1500 rpm for 60 min. Next, refinement was performed using a planetary ball mill operated at a parameter of 300 rpm for 2 h with a controlled ball to feed ratio of 10:1. The composite powders were analyzed by particle size analysis using a Horiba LA-960 Laser Particle Sizer (Horiba., Shanghai, China). All the particle size tests were repeated three times, and the results showed a reproducibility error of less than 1%.

2.2. Experimental Apparatus and Procedures

Figure 1 depicts the closed visualization apparatus utilized for gas deflagration and suppression experiments. The configuration integrates five essential subsystems: (1) a gas-fuel premixed deflagration chamber (140 mm $\times$ 140 mm $\times$ 700 mm), (2) a powder dispersion mechanism, (3) a high-frequency pulse ignition apparatus, (4) a rapid-imaging documentation setup, and (5) a high-resolution pressure monitoring assembly. The deflagration chamber is fabricated from steel to maximize containment integrity and withstand explosion pressures. The powder dispersion mechanism encompasses a nozzle, particulate reservoir, and electromagnetic control valve. The ignition apparatus employs an electric discharge to trigger premixed deflagration, featuring copper electrodes (0.1 mm diameter) with a 2 mm gap, energized by a pulsed DC generator operating at 0.5 kV. The imaging system incorporates a Phantom® VEO 710 camera interfaced with a computer operating Phantom Camera Control (v3.9) software, enabling comprehensive visualization of flame propagation dynamics at 4000 frames per second. The pressure monitoring assembly combines a data acquisition unit (Blast-PRO model with 4 MHz sampling capability) and a transducer (PCB-113B28 model with detection range of 0–344.7 kPa, temporal response $\leq$ 1 μs, and precision error of 0.1%). The transducer is situated 200 mm from the chamber's left boundary. RetryClaude can make mistakes. Please double-check responses.

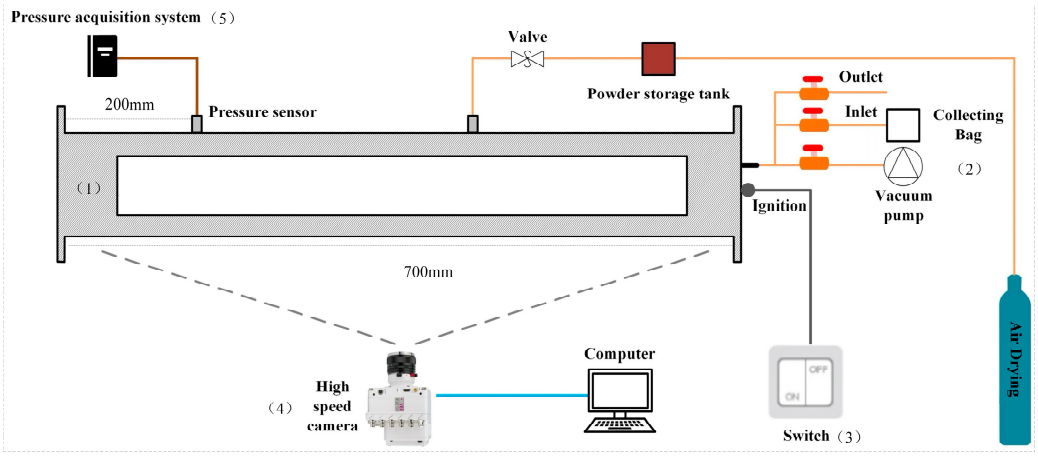


Figure 1. Schematic of the experimental system.

The experiments were carried out using a hydrogen/methane/air mixture with an equivalence ratio of 1.0 and a hydrogen content of 20 per cent. In order to investigate the effect of $Fe(C_5H_5)_2$ on the explosive behavior of hydrogen/methane/air mixtures, the $Fe(C_5H_5)_2$:SiO_2 mass ratios were formulated as (a) 0%:100%, (b) 2%:98%, (c) 4%:96%, and (d) 6%:94%, thereby creating a progressive concentration series. The hydrogen fraction X_{H_2} was defined by Wang et al. [22].

$$X_{H_2} = \frac{V_{H_2}}{V_{CH_4} + V_{H_2}}$$

Inject the gases into the gas storage bag according to the calculated proportions. The gases include methane, hydrogen, and air, and the purity of methane and hydrogen used in the experiment is 99.99 mass percent. After pumping the pipeline to a vacuum by means of a vacuum pump, the air collection bag is connected and the valve is opened to complete the inflation, after which, the valve is closed. Remove the gas bag, open the valve, and ventilate to atmospheric pressure. Let stand for 5 min. After completing the leak test, ignite the mixture using a spark igniter. Repeat each test at least 3 times to ensure the accuracy of the experimental results. After completing the experiment, to ensure that the next set of experiments is not affected, evacuate, open the valve to return to atmospheric pressure, and repeat more than 3 times.

2.3. Numerical Simulation

Homogeneous 0-D Reactor Models in Chemkin Pro were used to simulate the concentration distributions of key species, product formation rates, and temperature sensitivity of hydrogen/methane/air system at an initial temperature of 1300 K and a pressure of 1.0 atmosphere. The full chemical kinetic model used to simulate concentration distributions in doped hydrogen/methane/air explosions consists of 409 reactions and 104 substances. It consists of two sub-mechanisms: the GRI-Mech 3.0 mechanism for hydrogen and methane oxidation and the iron-based additive fire-extinguishing mechanism [23–28].

3. Results and Discussion

3.1. Effects on Flame Structure

Figure 2 illustrates the effect of different proportions of CDP on the flame propagation structure during natural gas explosions. As shown in Figure 2a, due to the confined space in the pipeline, the flame shape changes under wall constraints, resulting in an irregular elliptical shape between 10 and 30 ms. During the 30–40 ms period, the flame propagation slows down due to the influence of backflow, and the curvature of the flame front decreases,

gradually forming a nearly planar shape in the direction of propagation. However, after passing through the nozzle, the flame flow transforms into a turbulent state, with the flame propagation speed near the upper wall accelerating, eventually forming an inclined surface until it reaches the end of the pipeline. Compared to the case without powder, the mass fraction of 0%, 2%, 4%, and 6% $Fe(C_5H_5)_2$ composite powder delayed the flame arrival at the end of the pipeline by 51.43%, 48.57%, 71.43%, and 85.71%, respectively. The composite powder dispersed in the pipe intensified the turbulence, causing the flame to deform and wrinkle. As the flame propagated to the left, the composite powder absorbed the reaction heat slowed the speed of the flame. Under high temperatures, inerting decomposed, generating $C_5H_5\bullet$ and $FeC_5H_5\bullet$, which reacted with critical flame radicals such as •OH and •O, reducing the concentration of active radicals in the flame [13]. Additionally, $FeC_5H_5\bullet$ was further decomposed to form Fe•, consuming a significant number of free radicals, resulting in the formation of stable $Fe(OH)_2$, thereby inhibiting the explosive combustion reactions. It was observed that with increasing $Fe(C_5H_5)_2$ content in the composite powder, the flame propagation speed decreased, and the flame became brighter. This was found to be due to the destruction of •H and •OH in the flame, changing the flame color from orange to bright yellow [29]. Figure 3 shows the effect of different mass fractions of CDP on the flame propagation structure in hydrogen-enriched natural gas explosions. The flame propagation structure is similar to X_{H_2} = 0%. After adding the composite powder, the time for the flame to reach the end of the pipeline was extended by 23.08%, 53.85%, 38.46%, and 30.8%, respectively. This may be attributed to the fact that hydrogen addition to methane increases the laminar burning velocity of the premixed flame, leading to a faster flame front speed, which weakens the inerting effect of the composite powder. Nonetheless, CDP exhibits a significant inhibitory effect on the flame propagation of combustible gases, with the suppression effect increasing as the $Fe(C_5H_5)_2$ mass fraction in the composite powder increases. Figure 3 shows the effect of different mass fractions of CDP on the flame propagation structure in X_{H_2} = 20% explosions. The flame propagation structure is similar to X_{H_2} = 0%. After adding the composite powder, the time for the flame to reach the end of the pipeline was extended by 23.08%, 53.85%, 38.46%, and 30.8%, respectively. This may be attributed to the fact that hydrogen addition to methane increases the laminar burning velocity of the premixed flame, leading to a faster flame front speed, which weakens the inerting effect of CDP. Nonetheless, CDP exhibits a significant inhibitory effect on the flame propagation of combustible gases, with the suppression effect increasing as the $Fe(C_5H_5)_2$ mass ratios in the CDP increase.

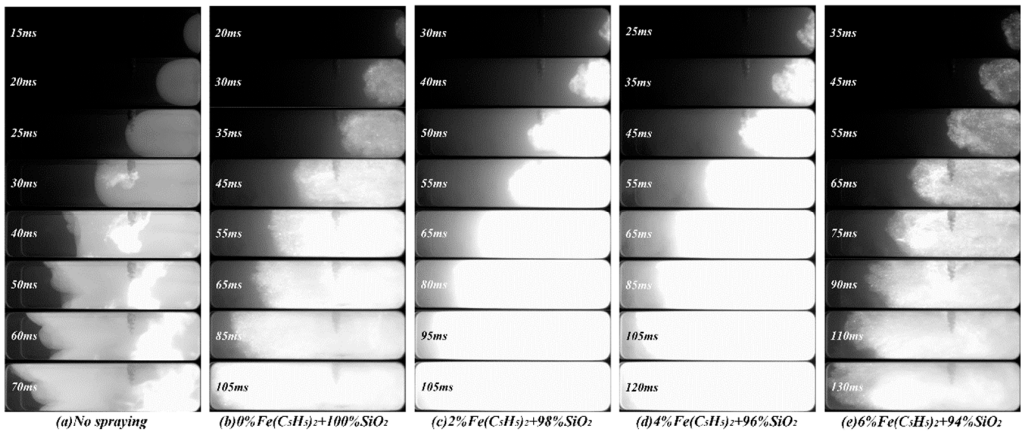


Figure 2. Variation of flame structure with X_{H_2} = 0% for different spraying and discharging scenarios.

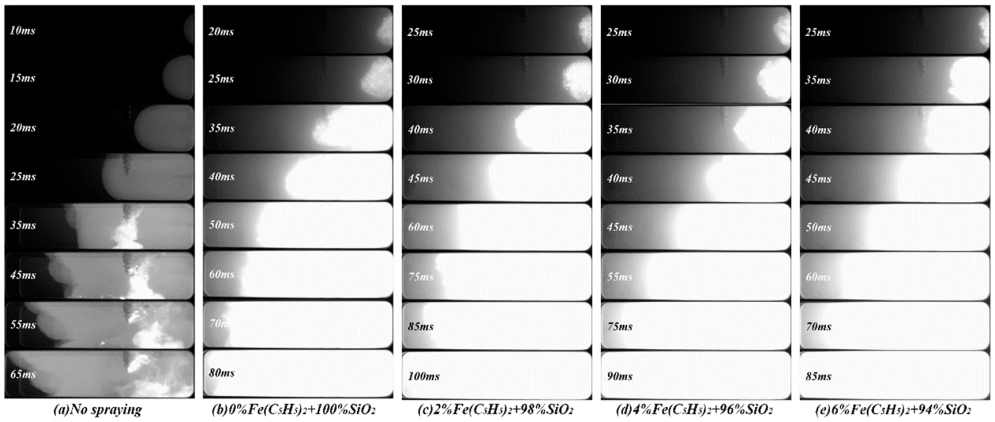


Figure 3. Variation of flame structure with X_{H_2} = 20% for different spraying and discharging scenarios.

3.2. Effects on Flame Propagation Velocity

To further investigate the flame propagation process under various conditions, Figure 4 illustrates the effect of different proportions of CDP on flame propagation speed during natural gas explosions. In Figure 4a, for X_{H_2} = 0%, the flame propagation speed peaked 15.721 m/s at 25 ms. Adding 100% SiO_2, the speed dropped to 13.744 m/s, with the peak speed delayed to 35 ms. Increasing the $Fe(C_5H_5)_2$ mass fraction further reduced the speed; at 6% $Fe(C_5H_5)_2$, the maximum speed decreased by 41.2% to 9.241 m/s, demonstrating the most effective inhibition. This indicates that $Fe(C_5H_5)_2$ significantly reduces flame propagation speed in methane explosions. Figure 4b presents the results for X_{H_2} = 20%. Without inhibitors, the flame speed peaked at 17.142 m/s, higher than for pure methane. This suggests that hydrogen accelerates flame propagation due to its high laminar burning velocity and rapid heat release [30]. Adding the CDP reduced flame speed, though the suppression was less effective compared to that of pure methane. This difference arises because hydrogen, with its higher diffusion coefficient and faster combustion rate, alters the flame's chemical reaction mechanisms. Notably, with 4% $Fe(C_5H_5)_2$, the flame propagation speed slightly increased to 16.094 m/s, likely due to hydrogen weakening the $Fe(C_5H_5)_2$ suppression effect, possibly through secondary reactions that promote combustion. In hydrogen/methane flames, the faster burning velocities likely reduce the ability of $Fe(C_5H_5)_2$ to capture radicals, making inhibition less effective [31]. Overall, $Fe(C_5H_5)_2$ composites significantly suppress flame speed in methane explosions by capturing radicals and reducing reactive species. However, in X_{H_2} = 20%, the suppression effect is weaker, as hydrogen's rapid combustion properties alter flame propagation dynamics.

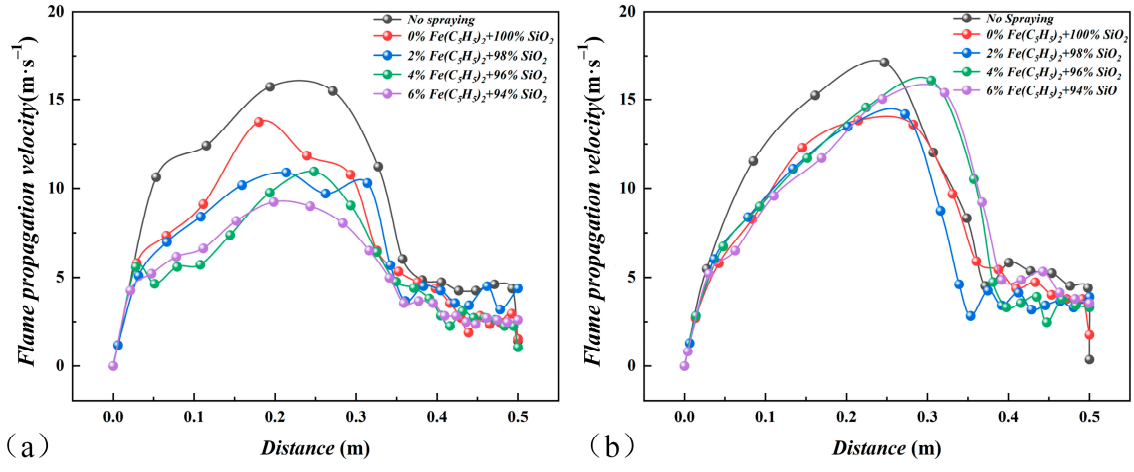


Figure 4. Variation of flame propagation velocity for different spraying scenarios: (**a**) X_{H_2} = 0%; (**b**) X_{H_2} = 20%.

3.3. Effects on Pressure Propagation

Figure 5 illustrates the effect of different mass fraction of CDP on the pressure curve of methane explosion under X_{H_2} = 0%. The maximum explosion pressure generally decreases as $Fe(C_5H_5)_2$ mass fraction increases. In the absence of inhibitors, the maximum pressure for pure methane reaches 0.564 MPa. Adding 4% $Fe(C_5H_5)_2$ and 96% SiO_2 reduces the maximum pressure to 0.505 MPa, a 10.5% reduction, showing the best inhibitory effect. However, further increasing $Fe(C_5H_5)_2$ to 6% leads to a slight rebound in pressure to 0.518 MPa, suggesting a saturation point in suppression effectiveness. Under X_{H_2} = 20%, the maximum pressure without inhibitors is 0.569 MPa, slightly higher than for pure methane, indicating that hydrogen increases explosion pressure. With inhibitors, the pressure gradually decreases, and 6% $Fe(C_5H_5)_2$ reduces the pressure to 0.525 MPa, a 7.7% reduction. This suggests that higher $Fe(C_5H_5)_2$ content is needed for similar inhibition under hydrogen conditions. The delay in explosion time is attributed to SiO_2 absorbing heat, lowering flame temperature, and diluting the gas. $Fe(C_5H_5)_2$ also decomposes, capturing radicals to interrupt the combustion chain [31]. These effects together slow flame propagation and reduce explosion pressure. $Fe(C_5H_5)_2$ composites effectively suppress both X_{H_2} = 0% and X_{H_2} = 20%, though the effect is slightly reduced with hydrogen addition.

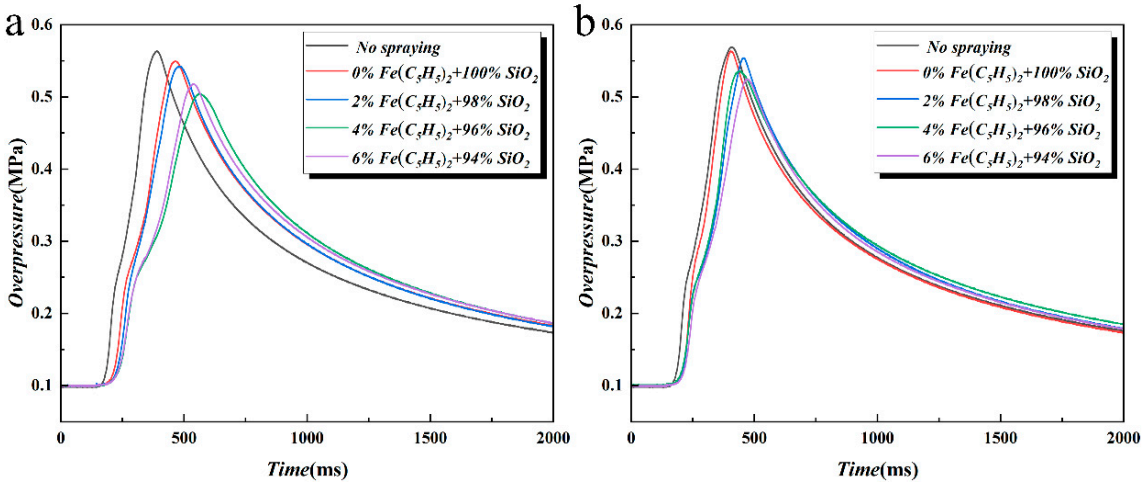


Figure 5. Variation of pressure propagation for different spraying cases: (**a**) X_{H_2} = 0%; (**b**) X_{H_2} = 20%.

3.4. Temperature Sensitivity Analysis

The essential reason for the increase in ambient pressure during the explosion is the transient release of energy, which can be characterized by the temperature change of the reaction system [32]. To evaluate the inhibitory effect of $Fe(C_5H_5)_2$ on premixed combustion explosions, a temperature sensitivity analysis of the main radical reaction was obtained, which characterizes the extent to which each step of the radical reaction affects the temperature change of the mixed system. As shown in Figure 6, for the analysis of the effect of added $Fe(C_5H_5)_2$ on the temperature sensitivity of pure methane combustion explosions, the reaction steps are mainly the first 10 primitive reactions with promoting or inhibiting rates. Positive values of temperature sensitivity indicate that the reaction promotes the temperature rise and negative values indicate that it inhibits the temperature rise. In the case of the primitive reactions with X_{H_2} = 0%, the main reactions promoting the temperature rise are R3 ($CH_3+O_2<=>OH+CH_2O$), R4 ($O_2+CH_2O<=>HO_2+HCO$), R4 ($O_2+CH_2O<=>HO_2+HCO$), R5 ($H+O_2<=>O+OH$), and R6 ($HO_2+CH_3<=>OH+CH_3O$), and the main reactions inhibiting the temperature rise are R7 ($2CH_3(+M)<=>C_2H_6(+M)$) and R8 ($H+CH_4<=>CH_3+H_2$). When $X_{Fe(C_5H_5)_2}$ = 2%, the reaction under the condition of R12 is the reaction of $Fe(C_5H_5)_2$ with HO_2, which is a one-way irreversible reaction that absorbs heat

and reduces the temperature of the reaction zone. HO_2 is consumed, so that the reactions R6 and R11 shown equilibrium inverse shift consumption of O_2 and the generation of CH_3 at the same time, due to the decrease in the concentration of O_2. For R2, R3, R4, and R5, the equilibrium positively shifted due to a lack of reactant. The concentration of CH_3 rises in the R8 inverse shift, and the mass fraction of $Fe(C_5H_5)_2$ increases; additionally, the sensitivity coefficients of the promoted reactions and R1, R2, R3, R4, R5, and R12 as well as the inhibited reaction R8 are gradually decreased.

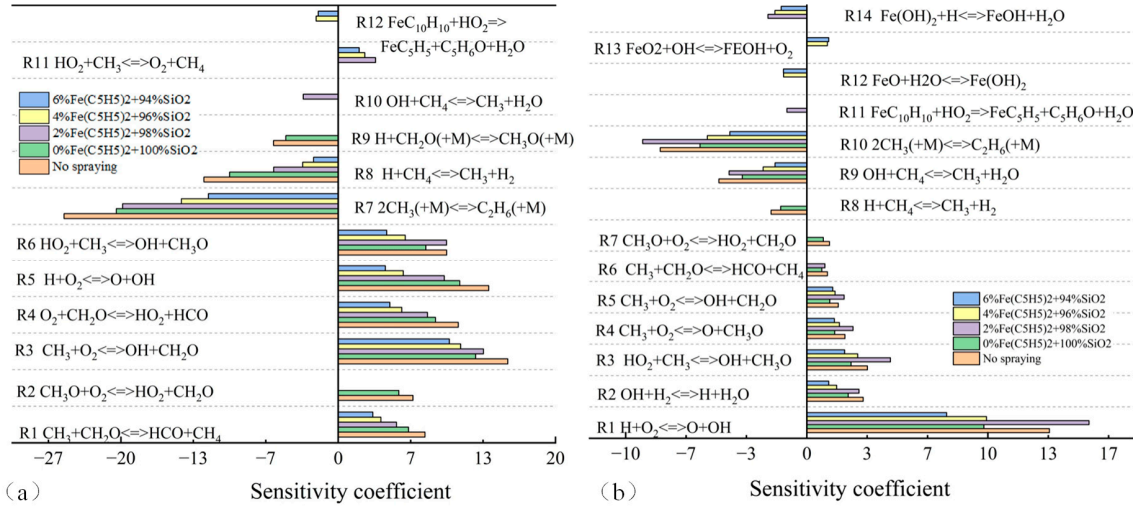


Figure 6. The Effect of SiO_2 with $Fe(C_5H_5)_2$ on the temperature sensitivity: ((**a**) $X_{H_2} = 0\%$; (**b**) $X_{H_2} = 20\%$).

For $X_{H_2} = 20\%$, the top 10 reactions for temperature sensitivity changed, and the temperature sensitivity coefficients for all reactions decreased compared to the $X_{H_2} = 0\%$ gas combustion reaction. The main reactions promoting the temperature increase became R1 ($H+O_2<=>O+OH$) and R3($HO_2+CH_3<=>OH+CH_3O$), and the main reactions inhibiting the temperature increase were R10($2CH_3(+M)<=>C_2H_6(+M)$) and R9 ($OH+CH_4<=>CH_3+H_2O$). For $Fe(C_5H_5)_2$-related reactions, the reactions inhibiting the temperature increase were R14 ($Fe(OH)_2+H<=>FeOH+H_2O$) and R12 ($FeO+H_2O<=>Fe(OH)_2$), and the reaction that promotes the temperature rise is R13 ($FeO_2+OH<=>FeOH+O_2$). It is noteworthy that the reaction under $X_{H_2} = 20\%$ conditions enhanced the temperature sensitivity coefficient of all radical reactions associated with $X_{Fe(C_5H_5)_2}$ = 2%. In the condition at $X_{Fe(C_5H_5)_2}$ = 2%, R11 ($FeC_{10}H_{10}+HO_2 <=>H_2O+ C_5H_6O+H_2O$) shows a suppressive effect for temperature. This is consistent with the experimental phenomenon in the previous section, where the flame propagation rate decreases the most under this condition, and the experimental and numerical simulation results are able to match the results.

Overall, the above sensitivity analysis well explains the inhibition process of $Fe(C_5H_5)_2$ in the hydrogen/methane/air combustion system. First, as shown in Figure 6, the addition of $Fe(C_5H_5)_2$ mitigated the reactive concentration of reactive •H radicals, thus slowing down the chain reaction of combustion. Moreover, $Fe(C_5H_5)_2$ was less involved in the inhibition of the temperature rise in the combustion reaction under the condition of $X_{H_2} = 0\%$, only for R12, but it also showed an inhibition effect on the temperature rise after the addition of $Fe(C_5H_5)_2$. When H_2 is involved in the reaction, both R11 and R14 show the inhibition effect on the temperature rise, and the negative sensitivity coefficient of the Fe-containing reactions gradually increases and the positive sensitivity coefficient gradually decreases, which indicates that $Fe(C_5H_5)_2$ has a better inhibition effect on the combustion under the condition of hydrogen doping.

3.5. Rate of Production for Key Radicals

This study has demonstrated that the mole fraction of reactive radicals (•H, •O, and •OH) plays a dominant role in the combustion process. Therefore, in order to better understand the effect of $Fe(C_5H_5)_2$ on the key free radicals (•H, •O, and •OH) in the hydrogen/methane/air deflagration process, it is valuable to study the effect of $Fe(C_5H_5)_2$ on the concentration of these key radicals. To investigate the effect of the addition of $Fe(C_5H_5)_2$ mass ratios, further analysis was carried out to obtain Figures 7 and 8, which show the effect of the addition of different mass fractions of $Fe(C_5H_5)_2$ on the rates of •H, •O, and •OH production for the conditions of $X_{H_2} = 0\%$ and $X_{H_2} = 20\%$, respectively. The numerical simulation results showed that for the $X_{H_2} = 0\%$ condition, the concentrations of •H, •O and •OH decreased gradually with the increase of $Fe(C_5H_5)_2$ mass fraction. As can be seen from Figure 7a, the decrease in •H was the largest, and with every 2% increase, the yield of •H decreased by 15–18%, and when $X_{Fe(C_5H_5)_2}$ was increased from 2% to 6%, the •H yield decreased from 0.0142 mole/cm^3·s^{-1} to 0.0096 mole/cm^3·s^{-1}. •O and •OH yields also showed different degrees of decrease when $X_{Fe(C_5H_5)_2}$ was increased from 2% to 6%; the yields of •O and •OH decreased by 35% and 18%, respectively. In addition, comparing the no-inhibitor addition condition with the $X_{Fe(C_5H_5)_2}$ = 0% condition, it is easy to find that silica only has a physical dilution effect on the overall combustion reaction. The same conclusion can be drawn for the $X_{H_2} = 20\%$ condition. •H decreased by 37.4% when $X_{Fe(C_5H_5)_2}$ was increased from 2% to 6%, and the yields of •O and •OH decreased by 36% and 20%, respectively. According to the above analysis and conclusion, it is known that $Fe(C_5H_5)_2$ has a chemical inhibition effect on the whole combustion reaction, which can produce a certain inhibition effect on the intermediate primitive reaction, so as to impede the chain reaction and reduce the temperature of the overall reaction process.

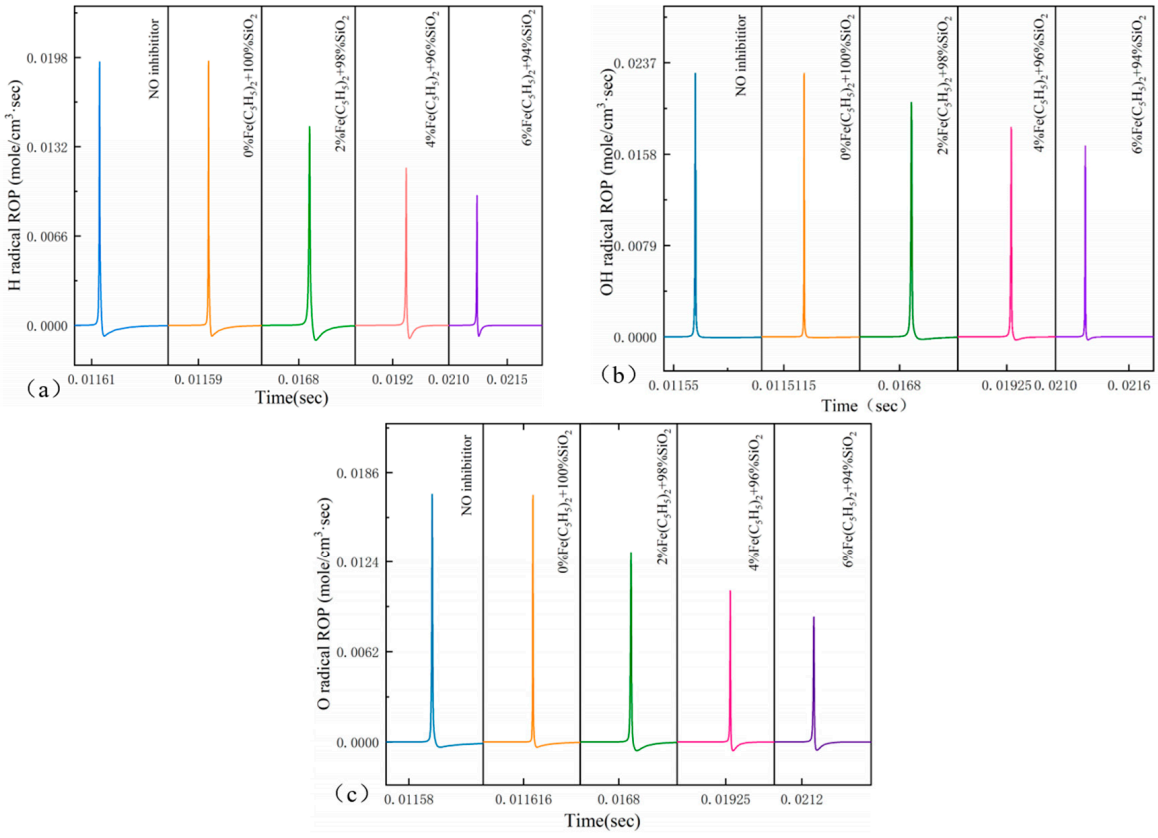


Figure 7. Main radicals rate of production for $X_{H_2} = 0\%$. (**a**) •H rate of production; (**b**) •OH rate of production; (**c**) •O rate of production.

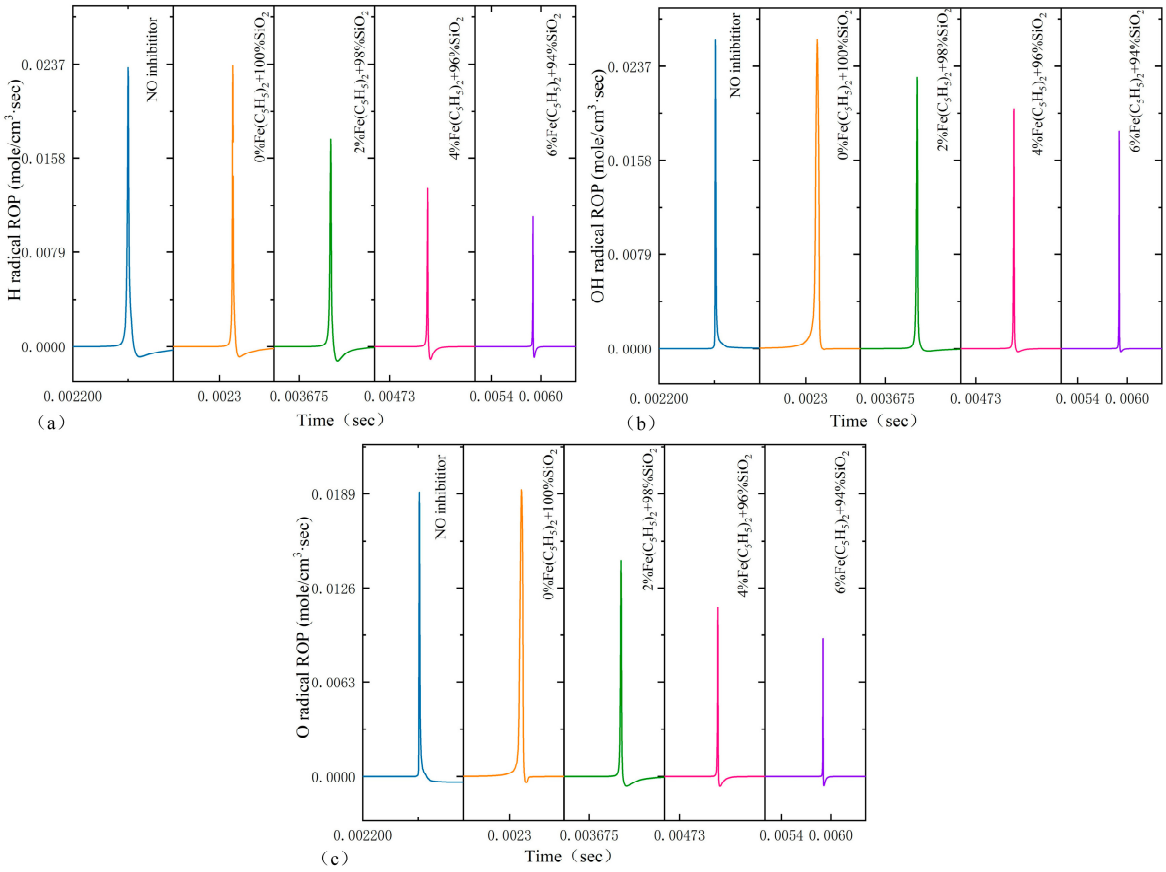


Figure 8. Main radicals rate of production for X_{H_2} = 20%. (**a**) •H rate of production; (**b**) •OH rate of production; (**c**) •O rate of production.

Figures 9 and 10 show the reaction process of the production and consumption of •H, •O, and •OH during the combustion explosion reaction of $Fe(C_5H_5)_2$ with methane/hydrogen/air mixtures, respectively. From Figures 9a and 10a, R1($OH+H_2<=>H+H_2O$), R5 ($O+CH_3<=>H+CH_2O$) and R6 ($OH+CO<=>H+CO_2$), for the entire combustion and explosion reaction, produce •H, and R10 ($H+O_2<=>O+OH$) is the consumption of •H of the main radical reaction. After the addition of $Fe(C_5H_5)_2$, R1($OH+H_2<=>H+H_2O$) for •H radical production decreased by about 30%. Because $Fe(C_5H_5)_2$ reacts with HO_2 to generate H_2O, H_2O is a product of R1, which will prevent the R1 equilibrium from shifting positively, reducing the yield of •H. As shown in Figures 9b and 10b, the radical reaction with the highest contribution to the generation of •O is R1 ($H+O_2<=>O+OH$), and the radical reactions with the highest contribution to the depletion of •O are R_2 ($O_2+CH<=>O+HCO$) and R3 ($C+O_2<=>O+CO$). The decrease in the •H radical yield after the addition of $Fe(C_5H_5)_2$ leads to a decrease in the rate of equilibrium forward movement due to the lack of O_2 and •H in R1, which decreases the yield of •O and •OH; in the depletion reactions R7 and R9, the concentration of •H radicals decreases, the forward shift of equilibrium reaction consumes •O , which increases the contribution of depletion reaction, and the •O radical yield shows an overall decreasing trend. The main reactions of •OH radical production and consumption were R1 ($H+O_2<=>O+OH$) and R8 ($OH+H_2<=>H+H_2O$), R10 ($OH+CO<=>H+CO_2$), respectively, and the reaction of •OH radical production was reversed in R1 due to the decrease in •H yield. Radicals in the reverse direction, R8 and R10, consume the reaction equilibrium in the positive direction with an increased contribution. For the reactions of •H, •O, and •OH, the addition of $Fe(C_5H_5)_2$ decreases the reaction rate of radical generation and increases the reaction rate of radical consumption.

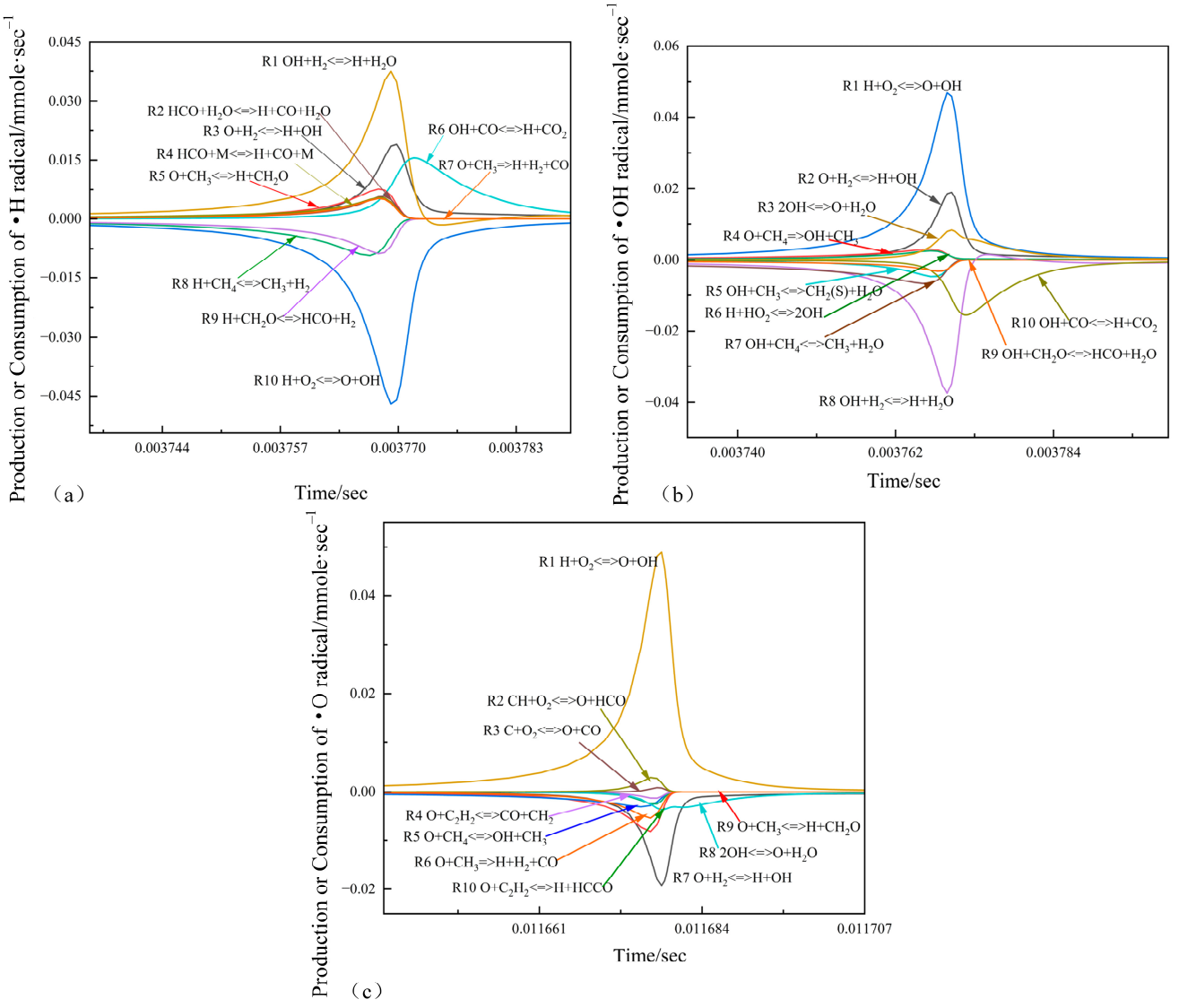


Figure 9. Rate of main radicals production for elementary reactions at X_{H_2} = 0%. (**a**) The production and consumption rate of •H; (**b**) The production and consumption rate of •OH. (**c**) The production and consumption rate of •O.

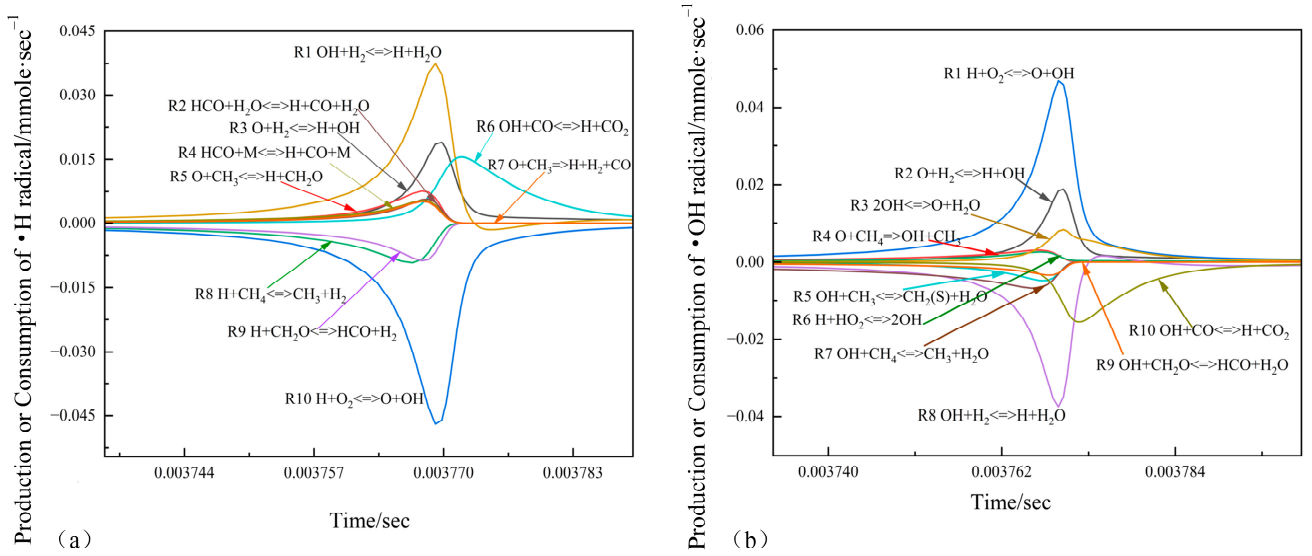


Figure 10. *Cont.*

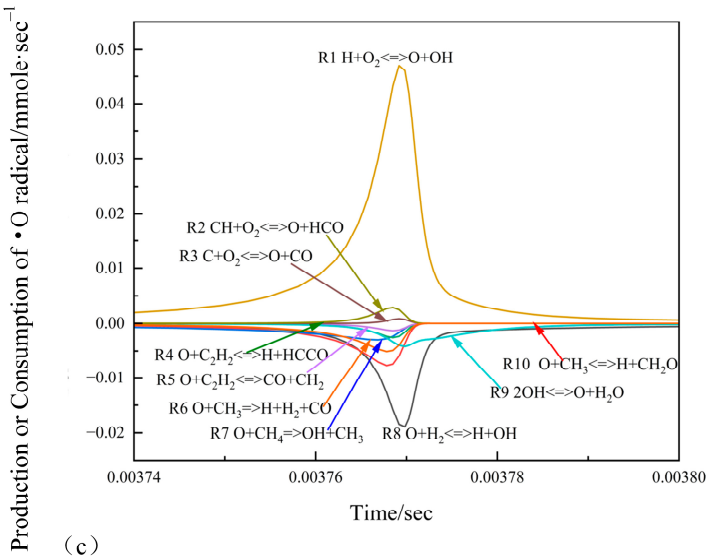


Figure 10. Rate of main radicals production for elementary reactions at X_{H_2} = 20%. (**a**) The production and consumption rate of •H; (**b**) The production and consumption rate of •OH. (**c**) The production and consumption rate of •O.

4. Conclusions

In this study, the effect of $Fe(C_5H_5)_2$-SiO_2 composite dry powder on the explosion of pure methane as well as hydrogen/methane/air mixtures was investigated experimentally and by simulation, and the main conclusions are as follows:

The incorporation of CDP significantly inhibited both flame propagation structure and velocity. Specifically, flame progression to the pipe's end was delayed, while propagation stability decreased, resulting in enhanced turbulence that led to flame distortion and wrinkling. Consequently, the flame morphology transformed from an irregular ellipse to an inclined surface. At X_{H_2} = 0%, the maximum flame propagation velocity decreased progressively with increasing the $Fe(C_5H_5)_2$ mass fraction compared to the 100% SiO_2 baseline. When $Fe(C_5H_5)_2$ reached 6% mass fraction, the maximum velocity decreased by 41.2% to 9.241 m/s, demonstrating an optimal suppression effect. In X_{H_2} = 20%, the addition of 2% $Fe(C_5H_5)_2$ effectively reduced flame propagation velocity compared to 100% SiO_2. However, the inhibition efficacy diminished significantly as the $Fe(C_5H_5)_2$ mass fraction increased beyond this point.

SiO_2 inhibited the combustion reaction only by physical dilution. $Fe(C_5H_5)_2$ showed significant chemical inhibition. Experiments showed that the maximum explosion pressure tended to decrease significantly as the mass fraction of $Fe(C_5H_5)_2$ increased. At X_{H_2} = 0%, 4% $Fe(C_5H_5)_2$ and 96% SiO_2 synergistically reduced the maximum pressure to 0.505 MPa (10.5%); at X_{H_2} = 20%, 6% $Fe(C_5H_5)_2$ was required to reduce the pressure to 0.525 MPa (7.7%), which was attributed to the physicochemical properties of hydrogen gas, which required a higher concentration of $Fe(C_5H_5)_2$ to achieve equivalent inhibition.

In the numerical study, the above sensitivity analysis explains the complete inhibition process of $Fe(C_5H_5)_2$ well in the hydrogen/methane/air and methane/air combustion system. Fe-based functional groups are directly involved in the combustion reaction system, markedly affecting its thermal sensitivity characteristics. From the key free radicals (•H, •O, and •OH) perspective, at the X_{H_2} = 0% condition, •H decreased by 0.0152 mole/cm^3·s^{-1} (33%), $X_{Fe(C_5H_5)_2}$ was increased from 2% to 6%, and the yields of •O and •OH decreased by 0.0223 mole/cm^3·s^{-1} (35%) and 0.0157 mole/cm^3·s^{-1} (18%). The same conclusion can be drawn for the X_{H_2} = 20% condition, •H, which decreased by 0.0196 mole/cm^3·s^{-1} (37.4%) when $X_{Fe(C_5H_5)_2}$ was increased from 2% to 6%, and the yields of •O and •OH decreased by

0.0095 mole/$cm^3 \cdot s^{-1}$ (36%) and 0.0218 mole/$cm^3 \cdot s^{-1}$ (20%), respectively. This suggests that $Fe(C_5H_5)_2$ contributes chemically to the combustion suppression mechanism.

Supplementary Materials: The following supporting information can be downloaded at: https://www.mdpi.com/article/10.3390/fire8050198/s1, Figure S1: Particle Size Distribution; Figure S2: Mechanism Schematic.

Author Contributions: Software, H.L.; Investigation, Y.L. and N.L.; Resources, Y.R.; Data curation, K.L.; Writing—original draft, Z.Z.; Visualization, H.Z.; Supervision, Z.L.; Project administration, H.M.; Funding acquisition, W.X. All authors have read and agreed to the published version of the manuscript.

Funding: This work was supported by the National Natural Science Foundation of China (NSFC 52274177, 51704054), Natural Science Foundation of Chongqing Scientific and Technological (CSTB2023NSCQ-MSX0862).

Data Availability Statement: The original contributions presented in this study are included in the article/Supplementary Materials. Further inquiries can be directed to the corresponding author.

Conflicts of Interest: Authors Yanhui Ren and Wei Xia were employed by the company PetroChina Company Limited. The remaining authors declare that the research was conducted in the absence of any commercial or financial relationships that could be construed as a potential conflict of interest.

References

1. Lee, J.E.; Jeon, K.J.; Show, P.L.; Lee, I.H.; Jung, S.C.; Choi, Y.J.; Rhee, G.H.; Lin, K.Y.; Park, Y.K. Mini review on H_2 production from electrochemical water splitting according to special nanostructured morphology of electrocatalysts. *Fuel* **2022**, *308*, 122048. [CrossRef]
2. Zhang, J.; Zhu, X.; Guo, Y.; Teng, Y.; Liu, M.; Li, Q.; Wang, Q.; Wang, C. Numerical Study of Homogenous/Inhomogeneous Hydrogen–Air Explosion in a Long Closed Channel. *Fire* **2024**, *7*, 418. [CrossRef]
3. Ban, J.; Zhu, L.; Shen, R.; Yang, W.; Hao, M.; Liu, G.; Wang, X. Research on hydrogen distribution characteristics in town hydrogen-doped methane pipeline. *Sci. Rep.* **2024**, *14*, 20347. [CrossRef]
4. Li, R.; Luo, Z.; Wang, T.; Cheng, F.; Lin, H.; Zhu, X. Effect of initial temperature and H_2 addition on explosion characteristics of H_2-poor/CH_4/air mixtures. *Energy* **2020**, *213*, 118979. [CrossRef]
5. Su, B.; Luo, Z.; Wang, T.; Xie, C.; Cheng, F. Chemical kinetic behaviors at the chain initiation stage of CH_4/H_2/air mixture. *J. Hazard. Mater.* **2020**, *403*, 123680. [CrossRef]
6. Mi, H.; Luo, N.; Shao, P.; Yi, H.; Wang, S.; Wang, W.; Niu, Y.; Yang, A.; Jiang, X.; Feng, Y.; et al. Interactive mechanisms of CF_3CHFCF_3 with H_2-CH_4-air mixture explosion: A synergistic study using chemical kinetic simulation and density functional theory. *Fuel* **2025**, *381*, 133603. [CrossRef]
7. Sun, Y.; Yuan, B.; Chen, X.; Li, K.; Wang, L.; Yun, Y.; Fan, A. Suppression of methane/air explosion by kaolinite-based multi-component inhibitor. *Powder Technol.* **2018**, *343*, 279–286. [CrossRef]
8. Liang, X.; Zhou, X.; Lu, X.; Liu, A. Investigation on slag resource utilization: $KHCO_3$/modified slag composite powder applied to methane/air explosion suppression. *Powder Technol.* **2024**, *441*, 119814. [CrossRef]
9. Xiao, Q.; Meng, X.; Li, Z.; Ma, X.; Yan, K.; Wang, Z. Inhibition of aluminum-silicon alloy dust explosion and flame by KH_2PO_4/montmorillonite composite powder. *Fire Mater.* **2022**, *46*, 797–808. [CrossRef]
10. Krasnyansky, M. Prevention and suppression of explosions in gas-air and dust-air mixtures using powder aerosol-inhibitor. *J. Loss Prev. Process Ind.* **2006**, *19*, 729–735. [CrossRef]
11. Yu, M.; Wang, X.; Zheng, K.; Han, S. Experimental investigation of gas explosion suppression by catalytic composite powder inhibitor. *J. China Coal Soc.* **2021**, *46*, 3212–3220.
12. Jia, J.; Tian, X. Experimental study on inhibiting methane-coal dust explosion by APP-diatomite composite explosion suppressant in the pipe network. *Arab. J. Chem.* **2024**, *17*, 105977. [CrossRef]
13. Yan, C.; Pan, X.; Hua, M.; Li, S.; Guo, X.; Zhang, C. Study on the fire extinguishing efficiency and mechanism of composite superfine dry powder containing ferrocene. *Fire Saf. J.* **2022**, *130*, 103606. [CrossRef]
14. Babushok, V.; Tsang, W. Inhibitor rankings for alkane combustion. *Combust. Flame* **2000**, *123*, 488–506. [CrossRef]
15. Linteris, G.T.; Rumminger, M.D.; Babushok, V.; Tsang, W. Flame inhibition by ferrocene and blends of inert and catalytic agents. *Proc. Combust. Inst.* **2000**, *28*, 2965–2972. [CrossRef]

16. Rumminger, M.D.; Reinelt, D.; Babushok, V.; Linteris, G.T. Inhibition of flames by iron pentacarbonyl. In Proceedings of the Halon Options Technical Working Conference, Albuquerque, NM, USA, 12–14 May 1998; pp. 145–156.
17. Reinelt, D.; Linteris, G.T. Experimental study of the flame inhibition effect of iron pentacarbonyl. In Proceedings of the Halon Options Technical Working Conference, Albuquerque, NM, USA, 7–9 May 1996.
18. Rausch, M.; Vogel, M.; Rosenberg, H. Ferrocene: A novel organometallic compound. *J. Chem. Educ.* **1957**, *34*, 268. [CrossRef]
19. Howard, J.B.; Kausch, W.J., Jr. Soot control by fuel additives. *Prog. Energy Combust. Sci.* **1980**, *6*, 263–276. [CrossRef]
20. Kasper, M.; Siegmann, K. The influence of ferrocene on PAH synthesis in acetylene and methane diffusion flames. *Combust. Sci. Technol.* **1998**, *140*, 333–350. [CrossRef]
21. Kasper, M.; Sattler, K.; Siegmann, K.; Matter, U.; Siegmann, H. The influence of fuel additives on the formation of carbon during combustion. *J. Aerosol. Sci.* **1999**, *30*, 217–225. [CrossRef]
22. Wang, Z.H.; Weng, W.B.; He, Y.; Li, Z.S.; Cen, K.F. Effect of H_2/CO ratio and N_2/CO_2 dilution rate on laminar burning velocity of syngas investigated by direct measurement and simulation. *Fuel* **2015**, *141*, 285–292. [CrossRef]
23. Fenard, Y.; Song, H.; Dauphin, R.; Vanhove, G. An engine-relevant kinetic investigation into the anti-knock effect of organometallics through the example of ferrocene. *Proc. Combust. Inst.* **2019**, *37*, 547–554. [CrossRef]
24. Jensen, D.E.; Jones, G.A. Catalysis of radical recombination in flames by iron. *J. Chem. Phys.* **1974**, *60*, 3421–3425. [CrossRef]
25. Rumminger, M.D.; Reinelt, D.; Babushok, V.; Linteris, G. Numerical study of the inhibition of premixed and diffusion flames by iron pentacarbonyl. *Combust. Flame* **1999**, *116*, 207–219. [CrossRef]
26. Kellogg, C.B.; Irikura, K.K. Gas-Phase thermochemistry of iron oxides and hydroxides: Portrait of a super-efficient flame suppressant. *J. Phys. Chem. A* **1999**, *103*, 1150–1159. [CrossRef]
27. Vanpee, M.; Shirodkar, P.P. A study of flame inhibition by metal compounds. *Symp. (Int.) Combust.* **1979**, *17*, 787–795. [CrossRef]
28. Li, Z.; Zuo, Q. Experimental study on the inhibition characteristics of n-heptane pool fire by ferrocene. *Fire Sci. Technol.* **2010**, *29*, 752–754.
29. Wang, Q.; Sun, Y.; Jiang, J.; Deng, J.; Shu, C.-M.; Luo, Z.; Wang, Q. Inhibiting effects of gas–particle mixtures containing CO_2, $Mg(OH)_2$ particles, and $NH_4H_2PO_4$ particles on methane explosion in a 20-L closed vessel. *J. Loss Prev. Process Ind.* **2020**, *64*, 104082. [CrossRef]
30. Wei, C.; Li, H.; Luo, Z.; Wang, T.; Yu, Y.; Wu, M.; Qi, B.; Yu, M. Quantitative analysis of flame luminance and explosion pressure in liquefied petroleum gas explosion and inerting: Grey relation analysis and kinetic mechanisms. *Energy* **2024**, *304*, 132046. [CrossRef]
31. Bhattacharjee, A.; Rooj, A.; Roy, D.; Roy, M. Thermal Decomposition study of ferrocene [$(C_5H_5)_2Fe$]. *J. Exp. Phys.* **2014**, *2014*, 513268. [CrossRef]
32. Xiao, H.; Duan, Q.; Sun, J. Premixed flame propagation in hydrogen explosions. *Renew. Sustain. Energy Rev.* **2018**, *81*, 1988–2001. [CrossRef]

Disclaimer/Publisher's Note: The statements, opinions and data contained in all publications are solely those of the individual author(s) and contributor(s) and not of MDPI and/or the editor(s). MDPI and/or the editor(s) disclaim responsibility for any injury to people or property resulting from any ideas, methods, instructions or products referred to in the content.